# Directional Mechanical Impedance of the Human Ankle During Standing with Active Muscles

Guilherme A. Ribeiro, Lauren N. Knop, and Mo Rastgaar, Member, IEEE

Abstract—The directional mechanical impedance of the human ankle was identified from subjects in a standing posture with varying levels of muscle activity. The impedance modeled the different torque responses to angle perturbations about different axes of rotation. This work proposed a novel impedance model that incorporated the coupling between multiple degrees of freedom of the ankle and was validated theoretically and experimentally. The reconstructed torque had an average variance accounted above 94% across twelve subjects. In addition, the impedance varied between and within trials and this variation was explained by changes in the ankle states, i.e., the ankle angle, torque, and muscle activities. These results have implications in the design of new prostheses controllers and the understanding of the human ankle function.

### I. INTRODUCTION

Advancements in the design and control of powered prostheses can improve the quality of life for amputees. The use of lower extremity powered prostheses has been shown to reduce the metabolic cost during walking, and improve symmetry of gait and overall mobility of transtibial amputees [1]. Many of these devices inject energy during the stance phase of the gait cycle and have one or two degrees of freedom (DOF) [2]. One of the main challenges with such powered ankle-foot prostheses is to find the most efficient and preferably anthropomorphic ways to be controlled. Currently, these technologies do not incorporate most of the physiological and neuromuscular characteristics of an unimpaired ankle, which can hinder the user's mobility and lead to secondary injuries caused by an overcompensation of other joints [3].

One approach to address this challenge is to understand the physiological and neuromuscular characteristics from an unimpaired ankle, such as how the ankle angle, torque, or mechanical impedance modulate as a function of the contributing muscle activities. Several research groups have quantified the kinematic characteristics of the ankle across different phases of the gait cycle [4], [5], and for different gait speeds and inclinations [6]. However, most works focused on the sagittal plane.

Furthermore, the mechanical impedance of the ankle has been shown to depend on the direction of the ankle rotation [7]–[9], and respond nonlinearly to changes of muscle

\*Research supported by NSF, grant number 1921046 and 1923760.

G. A. Ribeiro is with the Polytechnic Institute, Purdue University, West Lafayette, IN 47907 USA (e-mail: garamizo@purdue.edu).

Lauren N. Knop is with the Polytechnic Institute, Purdue University, West Lafayette, IN 47907 USA (e-mail: lknopp@purdue.edu).

contraction [10]–[12], of mean ankle torque [13], [14], and of mean ankle angle [15], [16]. Quantifying how the ankle impedance and neuromuscular activity vary across different tasks could potentially lead to improved prostheses control.

The use of electromyography (EMG) signals could improve prostheses control by understanding the user's intention before performing a specific task. Preliminary work by our group used a similar dataset determined that up to 40% of the data showed a significant linear correlation between the ankle impedance and muscle activation level [17]. Additionally, the authors previously studied the feasibility of developing a generalized model by exploring various ankle impedance estimation methods, EMG feature extraction techniques, and regression algorithms [10], [18]. However, these works did not account for the impedance dependence to the ankle angle and torque.

The goal of this study is to use regression techniques to investigate the relationship between the directional ankle impedance and lower extremity muscle activation levels. The novel approach presented in this paper identifies the directional ankle impedance based on a mathematical model and explains the impedance variation between and within trials by correlating the impedance with variations of ankle angle, torque, and muscle contraction.

### II. METHODS

## A. Experimental Setup

Twelve male subjects participated in this experiment and self-reported to have no neuromuscular or biomechanical disorders. All subjects provided written consent to participate in the study, as approved by the Institutional Review Board. The average age, mass, and height of the subjects were  $27.9 \pm 3.5$  years,  $92.3 \pm 27.6$  kg, and  $180.3 \pm 6.7$  cm, respectively.

The experimental setup, as shown in Figure 1, was designed to estimate the anisotropic mechanical impedance of the ankle and the corresponding muscle activity of the lower extremity. A previously developed instrumented Vibrating Platform was selected for its ability to apply torque perturbations to the ankle about all axes within the sagittal and frontal planes [19]. This platform consisted of a 2-DOF Vibrating Platform, a force plate module (Kistler - 9260AA), and a motion capture camera

M. Rastgaar is with the Polytechnic Institute, Purdue University, West Lafayette, IN 47907 USA (phone: (765) 494-8634; e-mail: rastgaar@purdue.edu).

system (OptiTrack Prime 17W), containing eight cameras. Together, the force plate and motion capture cameras measured the resulting ground reaction forces, ground reaction torques, and motion of the shin, foot, and platform as perturbations were applied. A sampling rate of 350 Hz was selected for both systems.

Additionally, the lower extremity muscle activity was recorded using wireless EMG sensors (Delsys Trigno Wireless System), which were placed on tibialis anterior (TA), peroneus longus (PL), soleus (SOL), and gastrocnemius (GA). The measurements were sampled at 2000 Hz.

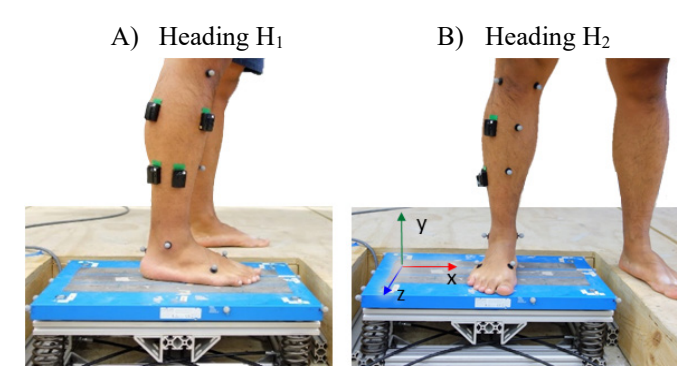


Fig. 1. Experimental setup while the subject stood in two heading positions. The Vibrating Platform, force plate module, motion capture camera reflective markers, and EMG sensors are shown.

### B. Experimental Protocol

First, the maximum voluntary contractions (MVC) of the subject's muscles were determined while in a standing posture. The subject maximally co-contracted the instrumented muscles for a one-second burst and repeated the burst approximately ten times. The highest voltage achieved by the TA muscle was selected as the MVC reference throughout the remainder of the experiment.

Next, a total of 10 trials were performed, each of which had a duration of 70 seconds. The subjects stood with legs shoulder-width apart, with their right foot placed on the vibrating force plate. The Vibrating Platform applied random torque perturbations around the X and Z axes shown in Fig. 1 (uniform distribution across actuation range) at a 30 Hz update rate. Using real-time feedback of the EMG sensors on a monitor, the subjects maintained their TA muscle activity to be relaxed or co-contracted to 10%, 20%, 30%, or 40% MVC for the duration of each trial, while the other muscles' activities were measured. The five trials were repeated twice while standing with a heading along the X axis (Fig. 1.A) and along the Z axis (Fig. 1.B) of the force plate coordinate system. All trials and headings were performed in a randomly selected order, and at least one minute of rest was considered between trials to limit the effects of muscle fatigue.

### C. Calibration of the Experimental Apparatus

The Vibrating Platform was designed to estimate the human kinematics without the influence of the actuators' dynamics. However, the experimental measurements are influenced by the inertial dynamics of the force plate, which is substantial compared to the foot inertia. Therefore, these dynamics were compensated on the measured forces and torques in the following procedure: 1) the equation of motion was modeled

as a function of the force plate kinematics and inertial parameters; 2) a calibration trial was performed in which the Vibrating Platform was actuated (without human subjects); 3) the inertial parameters of the force plate were estimated using the equation of motion and the experimental data, and finally 4) the inertial effects of the apparatus were compensated for human experiments.

A coordinate frame,  $\{P\}$ , is defined at the center of the force plate's top surface, with axes directions shown in Fig. 1. The measured forces and torques are taken with respect to this frame. The translational and rotational equations of motion were calculated from the linear momentum,  $p_P$ , and angular momentum,  $L_P$ , around the  $\{P\}$  origin, respectively:

$$\sum_{P} \mathbf{F} = \frac{d\mathbf{p}_{P}}{dt}$$

$$\mathbf{F}_{P} + m_{P}\mathbf{g} = \frac{d(m_{P}\dot{\mathbf{s}}_{P_{0}})}{dt}$$

$$\mathbf{F}_{P} = m_{P}(\ddot{\mathbf{s}}_{P_{0}} - \mathbf{g})$$

$$\sum_{P} \mathbf{\tau} = \frac{d\mathbf{L}_{P}}{dt}$$

$$\mathbf{\tau}_{P} + \mathbf{r}_{P} \times m_{P}\mathbf{g} = \frac{d(I_{P}\boldsymbol{\omega}_{P} + \mathbf{r}_{P} \times m_{P}\dot{\mathbf{s}}_{P_{0}})}{dt}$$

$$\mathbf{\tau}_{P} = I_{P}\dot{\boldsymbol{\omega}}_{P} + \boldsymbol{\omega}_{P} \times (I_{P}\boldsymbol{\omega}_{P})$$

$$+ \mathbf{r}_{P} \times m_{P}(\ddot{\mathbf{s}}_{P_{0}} - \mathbf{g}) + (\boldsymbol{\omega}_{P} \times \mathbf{r}_{P}) \times m_{P}\dot{\mathbf{s}}_{P}$$

$$(1)$$

where the linear velocity and acceleration of the force plate center of mass (CoM) are calculated, respectively, as

$$\dot{\mathbf{s}}_{P_0} = \dot{\mathbf{s}}_P + \boldsymbol{\omega}_P \times \boldsymbol{r}_P$$

$$\ddot{\mathbf{s}}_{P_0} = \ddot{\mathbf{s}}_P + \dot{\boldsymbol{\omega}}_P \times \boldsymbol{r}_P + \boldsymbol{\omega}_P \times (\boldsymbol{\omega}_P \times \boldsymbol{r}_P)$$
(3)

and  $F_P$ ,  $\tau_P$ , and g, are the measured force, measured torque, and gravity vector, respectively. The kinematic variables  $\dot{s}_P$ ,  $\ddot{s}_P$ ,  $\omega_P$ , and  $\dot{\omega}_P$  are the linear velocity, linear acceleration, angular velocity, and angular acceleration of the force plate frame, respectively. The inertial parameters  $m_P$ ,  $r_P$ , and  $l_P$  are the mass, CoM vector, and moment of inertia tensor of the force plate, respectively.

The set of unknown inertial parameters,  $\beta$ , of the force plate was estimated by minimizing the cost function,  $\varepsilon_{\beta}$ , via a nonlinear optimization method (MATLAB's *fmincon* function, interior-point algorithm [20]):

$$\beta^* \triangleq \underset{\beta}{\operatorname{argmin}} \sum_{t} \varepsilon_{\beta}[t]^T \varepsilon_{\beta}[t]$$

$$\operatorname{for} \varepsilon_{\beta}[t] \triangleq \begin{bmatrix} \boldsymbol{F}_{p}^{(\beta)}[t] - \boldsymbol{F}_{p}[t] \\ \boldsymbol{\tau}_{p}^{(\beta)}[t] - \boldsymbol{\tau}_{p}[t] \end{bmatrix}$$

$$\operatorname{and} \beta \triangleq \{m_{p}, \boldsymbol{r}_{p}, l_{p}\},$$

$$(4)$$

where  $F_p^{(\beta)}$  and  $\tau_p^{(\beta)}$  are the modeled force and torque dependent on the inertial parameters (as shown in (1) and (2)) and the operator [t] represents a measurement at time t. The time derivatives were calculated with a Sarvitzky-Golay filter [21] with a 15-sample window and a 5<sup>th</sup> order polynomial. This filter approximates the signal within a moving window as a

polynomial and calculates the time derivatives with noise rejection.

Finally, the inertial effects of the force plate during the experiments with the human subjects were determined and subtracted from the measured forces and torques using (1) and (2) with the force plate kinematics sampled during the human trials and the estimated inertial parameters.

### D. Directional Ankle Impedance

In this section, the ankle impedance was modeled as a direction-dependent, three-dimensional variable. A foot coordinate system,  $\{F\}$ , is fixed on the foot, with an origin on the ankle center, Y axis pointing upward and X axis pointing in the anterior-posterior direction (aligned with the foot's major axis). The ankle angle is the foot orientation with respect to the shank and is represented in the axis-angle notation

$$\boldsymbol{q} = \begin{bmatrix} q_x \\ q_y \\ q_z \end{bmatrix} = q\hat{\boldsymbol{v}} \tag{5}$$

where q is the magnitude of rotation and  $\widehat{v}$  is the axis of rotation. Assuming the ankle rotations in dorsiflexion-plantarflexion (DP,  $q_z$ ) and inversion-eversion (IE,  $q_x$ ) are much larger than in external-internal (EI,  $q_y$ ) since the Vibrating Platform does not rotate along the Y axis.

Suppose the tendons, tissues, and cartilage elasticity around the ankle act as infinitesimal angular springs along each rotation direction,  $\varphi$ , of the ankle. Because the stiffness of these springs has an arbitrary value, it was represented as a Fourier series with  $\varphi$  as the independent variable ( $\varphi$  for the dorsiflexion, inversion, plantarflexion, and eversion angles are  $0^{\circ}$ ,  $90^{\circ}$ ,  $180^{\circ}$ , and  $270^{\circ}$ , respectively).

$$dK(\varphi) = \frac{1}{2}K_0 + \sum_{i=1}^{\infty} \alpha_i \cos(2i\varphi) + \sum_{i=1}^{\infty} \beta_i \sin(2i\varphi) \quad (6)$$

where  $K_0$ ,  $\alpha_i$ , and  $\beta_i$  are the coefficients of the series. The angle displacement,  $\theta(\varphi)$ , of each infinitesimal spring generates a torque in an axis,  $\hat{u}(\varphi)$ :

$$\theta(\varphi) = q_x \sin\varphi + q_z \cos\varphi \tag{7}$$

$$\hat{\boldsymbol{u}}(\boldsymbol{\varphi}) = [\sin \boldsymbol{\varphi} \quad 0 \quad \cos \boldsymbol{\varphi}]^T \tag{8}$$

The net torque on the ankle is the sum of the torques from all the infinitesimal springs:

$$\tau_{K} = \int_{0}^{2\pi} dK(\varphi)\theta(\varphi)\hat{\boldsymbol{u}}(\varphi)d\varphi 
= \frac{\pi}{2} \begin{bmatrix} K_{0} - \alpha_{1} & 0 & \beta_{1} \\ 0 & 0 & 0 \\ \beta_{1} & 0 & K_{0} + \alpha_{1} \end{bmatrix} \boldsymbol{q} 
\tau_{K} = \begin{bmatrix} K_{X} & 0 & K_{XZ} \\ 0 & 0 & 0 \\ K_{YZ} & 0 & K_{Z} \end{bmatrix} \boldsymbol{q}$$
(9)

changing variables to  $K_x = \frac{\pi}{2}(K_0 - \alpha_1)$ ,  $K_z = \frac{\pi}{2}(K_0 + \alpha_1)$  and  $K_{xz} = \frac{\pi}{2}\beta_1$ . Note that the Fourier series coefficients for higher-order components were canceled in the integral

evaluation. In addition, (9) demonstrates that an anisotropic ankle impedance can generate a reaction torque in a different direction than the axis of ankle rotation due to the  $K_{xz}$  component.

For an ankle rotation  $\mathbf{q} = [q' \sin \varphi \ 0 \ q' \cos \varphi]^T$  with magnitude q' along direction  $\varphi$ , the torque component projected on the rotation plane is

$$\tau_{K}^{'} = \left[\sin\varphi \quad 0 \quad \cos\varphi\right] \begin{bmatrix} K_{x} & 0 & K_{xz} \\ 0 & 0 & 0 \\ K_{xz} & 0 & K_{z} \end{bmatrix} \begin{bmatrix} q'\sin\varphi \\ 0 \\ q'\cos\varphi \end{bmatrix} 
\tau_{K}^{'} = q' \left(\frac{K_{z} - K_{x}}{2}\cos2\varphi + \frac{K_{z} + K_{x}}{2} + K_{xz}\sin2\varphi\right)$$
(10)

The net ankle stiffness, *K*, along this plane of motion is the slope of the angle-torque curve, thus, calculated as

$$K(\varphi) = \frac{\partial \tau_{K}^{'}(q^{'})}{\partial q^{'}}$$

$$K(\varphi) = \frac{K_{z} - K_{x}}{2} \cos 2\varphi + \frac{K_{z} + K_{x}}{2} + K_{xz} \sin 2\varphi$$
(11)

Equation (11) shows that even though the stiffness of the infinitesimal springs could take an arbitrary shape, the net stiffness is constrained to a Fourier series of 1<sup>st</sup> order, with three free parameters,  $K_x$ ,  $K_{xz}$ , and  $K_z$ .

The same anisotropic model applied in the stiffness component modeling can be applied to the damping and inertia components. The total ankle impedance response is

$$\boldsymbol{\tau}_{Z}(\boldsymbol{q}, \dot{\boldsymbol{q}}, \ddot{\boldsymbol{q}}) = \begin{bmatrix} K_{x} & 0 & K_{xz} \\ 0 & 0 & 0 \\ K_{xz} & 0 & K_{z} \end{bmatrix} \boldsymbol{q} \\
+ \begin{bmatrix} B_{x} & 0 & B_{xz} \\ 0 & 0 & 0 \\ B_{xz} & 0 & B_{z} \end{bmatrix} \dot{\boldsymbol{q}} + \begin{bmatrix} J_{x} & 0 & J_{xz} \\ 0 & 0 & 0 \\ J_{xz} & 0 & J_{z} \end{bmatrix} \ddot{\boldsymbol{q}}$$
(12)

Next, this impedance model is added to the equation of motion of the ankle, which accounts for external torques and the inertia of the foot. From the angular momentum around the foot ankle:

$$\sum_{F} \boldsymbol{\tau} = \frac{d\boldsymbol{L}_{F}}{dt}$$

$$\boldsymbol{\tau} + \boldsymbol{r} \times m\boldsymbol{g} + \boldsymbol{\tau}_{Z}(\boldsymbol{q}, \dot{\boldsymbol{q}}, \ddot{\boldsymbol{q}}) = \frac{d(\boldsymbol{I}\boldsymbol{\omega} + \boldsymbol{r} \times m\dot{\boldsymbol{s}}_{0})}{dt}$$

$$\boldsymbol{\tau} = \boldsymbol{I}\dot{\boldsymbol{\omega}} + \boldsymbol{\omega} \times (\boldsymbol{I}\boldsymbol{\omega}) + \boldsymbol{r} \times m(\ddot{\boldsymbol{s}}_{0} - \boldsymbol{g})$$

$$+(\boldsymbol{\omega} \times \boldsymbol{r}) \times m\dot{\boldsymbol{s}} + \boldsymbol{\tau}_{Z}(\boldsymbol{q}, \dot{\boldsymbol{q}}, \ddot{\boldsymbol{q}})$$
(13)

where the linear velocity and acceleration of the foot CoM are respectively calculated as

$$\dot{\mathbf{s}}_0 = \dot{\mathbf{s}} + \boldsymbol{\omega} \times \boldsymbol{r}$$
$$\ddot{\mathbf{s}}_0 = \ddot{\mathbf{s}} + \dot{\boldsymbol{\omega}} \times \boldsymbol{r} + \boldsymbol{\omega} \times (\boldsymbol{\omega} \times \boldsymbol{r})$$
(14)

where  $\tau$  is the external torque acting on the ankle. The kinematic variables  $\dot{s}$ ,  $\ddot{s}$ ,  $\omega$ , and  $\dot{\omega}$  are the linear velocity, linear acceleration, angular velocity, and angular acceleration of the foot, respectively. The inertial parameters m, r, and I

are the mass, CoM vector, and moment of inertia tensor of the foot, respectively.

Equation (13) is reshaped to a matrix form to separate the impedance parameters in a column vector. The Y component of the torque was removed because the Vibrating Platform does not actuate in this direction.

where, for brevity,  $\mathbb{A}$  is the matrix of the kinematic signals and C is the vector of the regression coefficients from the foot inertia,  $C_1$  to  $C_6$ . Analyses about the C vector were not reported because this vector represents the physical inertia of the foot, which might be better estimated by other methods such as 3D scanning [22]. The impedance coefficients of the directional model are  $K_x$ ,  $K_{xz}$ ,  $K_z$ ,  $B_x$ ,  $B_{xz}$ ,  $B_z$ ,  $J_x$ ,  $J_{xz}$ , and  $J_z$ . The X and Z subscript represents the variables in the IE and DP directions, respectively, while the XZ variables represent the cross-axis relationship between the DP and IE axes.

The coefficients of the impedance model were calculated to best fit the experimental data to (15) via Least Square regression. The varying impedance was identified at each time  $t_i$  within a rolling time-window centered at time  $t_i$  (16). The window contained 701 samples (N = 300) to include 2 seconds of measurements. In addition, the angle and torque best-fit lines were removed within each window to reduce the effects of human motion artifacts. The impedance calculated from this model is referred to as identified impedance.

$$\begin{bmatrix}
\tau_{x}[t_{i-N}] \\
\tau_{z}[t_{i-N}] \\
\tau_{x}[t_{i-N+1}] \\
\tau_{z}[t_{i-N+1}] \\
\vdots \\
\tau_{x}[t_{i+N}] \\
\tau_{z}[t_{i+N}]
\end{bmatrix} = \begin{bmatrix}
\mathbb{A}[t_{i-N}] \\
\mathbb{A}[t_{i-N+1}] \\
\mathbb{A$$

where 2N + 1 is the window length, and the operator  $[t_j]$  represents a signal at the time  $t_i$ .

The time derivatives were calculated with a Sarvitzky-Golay filter [21] with a 15-sample window and a 5<sup>th</sup> order polynomial. In addition, the signals were bandpass filtered (finite impulse response based on a Hamming window, 100<sup>th</sup> order, passband from 3 to 20 Hz). The later filter reduces the

effects of the high-frequency sensor noise and the low-frequency human motion artifacts.

To test the accuracy of the model in reconstructing the external torque in (15), the Variance Accounted For (VAF) of the torque in IE and DP directions was calculated within the 2-second window:

$$VAF_{\hat{y}[t_i]} = 1 - \frac{var(y[t_{i-N:i+N}] - \hat{y}[t_{i-N:i+N}])}{var(y[t_{i-N:i+N}])}$$
(17)

where y and  $\hat{y}$  are the reference and estimated signals, respectively. The operator  $[t_{i-N:i+N}]$  represents a time-sequence from the time instant  $t_{i-N}$  to  $t_{i+N}$ .

# E. Explaining the Time-Varying Mechanical Impedance

To verify that the variations of the identified impedance across and within the trials are caused by changes of the ankle states rather than a bias error of the system identification method, a regression model was developed to explain the impedance variation as a function of the muscle activity, mean ankle angles, and mean torques. The impedance calculated from this regression model is referred to as correlated impedance.

A regression model was developed for each subject and for all nine impedance parameters using the following ten predictor variables: DP, IE, and EI mean ankle angles and torques, and TA, PL, SOL, and GA muscle contractions via EMG. The regression model was a Least Square model with quadratic terms, which contains an intercept term, linear and squared terms for each predictor, and all products of pairs of predictors. The muscle contraction predictors were calculated as the moving Median Absolute Deviation (MAD) of the four EMG measurements in a 2-second window. In addition, the predictors and the response were low-pass filtered (finite impulse response based on a Hamming window, 200th order, 1 Hz cutoff) to explain the impedance variations of low-frequencies rather than of higher frequencies.

The regression model was trained and validated using 90% and 10% of the samples across all ten trials, respectively. The validation consisted of calculating the Mean Absolute Error (MAE) of the impedance parameter using all available samples from the validation set. The impedance MAE was calculated with the validation dataset to verify that the model did not over-fit to the training set.

### III. RESULTS

# A. Vibrating Platform Dynamics

The inertial parameters of the force plate were determined prior to each experiment for all subject. The average and standard deviation of parameters and VAF were calculated across the twelve calibration tests. The moment of inertia, product of inertia, and CoM was  $[38.9 \pm 0.5, 145.9 \pm 1.1, 122.4 \pm 0.9]^T$  g.m²,  $[5.0 \pm 0.5, -0.7 \pm 0.3, 0.1 \pm 0.5]^T$  g.m², and  $[-2.9 \pm 1.2, -16.2 \pm 1.1, 4.9 \pm 0.8]$  mm, respectively. The VAFs of the torque and force were substantially high, at  $[97.7 \pm 0.5, 96.3 \pm 0.9, 98.3 \pm 0.4]$  % and  $[96.0 \pm 0.6, 84.2 \pm 2.3, 98.2 \pm 0.4]$  %, respectively.

The estimated inertia parameters were similar to that of a box with equivalent mass and shape, which have a moment of

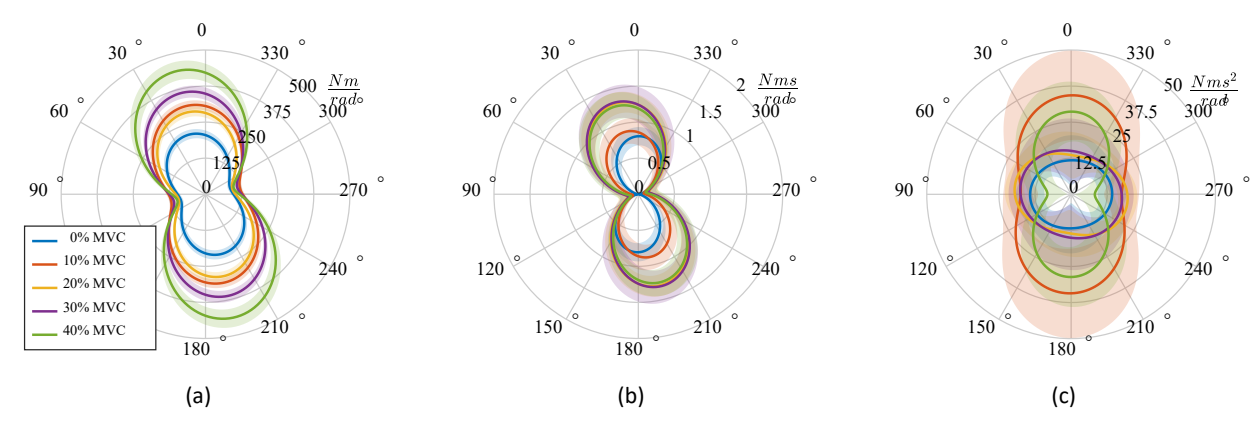


Fig. 2. Directional impedance as a function of the rotation direction and contraction levels of the TA muscle for a representative subject. (a) Stiffness, (b) damping, and (c) inertia parameters. The average (solid lines) and standard deviation (shaded region) of the identified impedance was calculated across trial. Dorsiflexion, inversion, plantarflexion, and eversion angles are represented by 0°, 90°, 180°, and 270°, respectively.

inertia, product of inertia, and CoM of [34.8, 131.2, 97.0]<sup>T</sup> g.m<sup>2</sup>, 0.0 g.m<sup>2</sup>, and [0, -14.4, 0] mm, respectively. This similarity indicates the mass distribution inside the force plate is fairly homogeneous. The VAF of the Y-axis force was lower than the other signals likely because the Vibrating Platform does not have an actuated translation in the up-down direction; thus, it has a lower signal to noise ratio on this direction. The high VAF, the small variance of the estimated inertial parameters and its similarity to the inertial parameters of a box indicate the parameter estimation was accurate, allowing for an unbiased characterization of the human ankle.

# B. Summary of the Ankle Impedance Characteristics

The ankle stiffness was larger along DP than along IE directions and resembled a "peanut" shape with a counter-clockwise rotation by around 0-30° (along dorsi-inversion). In addition, there was a higher modulation along the DP direction (Fig. 2), which is consistent with non-weight bearing ankle studied by Lee et al. [7], [8]. The magnitude of the identified standing ankle stiffness in this work was substantially larger (passive stiffness of 91.1±42.4 and 158.4±80.0 Nm/rad for IE and DP, respectively) when compared the non-weight bearing studies in [7], [8] (stiffness for 10% MVC SOL contraction was 13.7 and 45.3 Nm/rad, for IE and DP, respectively). In fact, the range of the identified stiffness and damping during standing were more similar to the results reported by Rouse et al [23], in which the impedance was estimated during walking.

In addition, in this work the stiffness increase 1.3 and 2 times, in IE and DP, respectively (between the passive and 30% MVC trials), while Lee et al. reported higher

modulation, increasing up to 5 and 9 times the value stiffness in IE and DP, respectively. This work also found that the damping increased 1.8 and 1.3 times; and the inertia increased 2.9 and 1.1 times, for DP and IE, respectively. The damping and inertia parameters showed a relatively lower inclination of the major axis. This can be verified by the cross-components (XZ) parameters closer to zero, relative to the X and Z components. This trend was observed for all trials, regardless of the heading of the subject. This indicates that the experimental apparatus did not substantially affect the behavior of the ankle.

For each subject, the identified ankle impedance was averaged across each trial, then averaged within trials of the same muscle contraction level. The mean and standard deviation across subjects of the mass-normalized impedance is presented in Table I. The average VAF for DP and IE torque across subjects and trials were  $94.0\pm3.2\%$  and  $95.7\pm2.8\%$ , respectively.

# C. Varying Ankle Impedance

The identified and correlated stiffness values from a representative subject are shown in Fig. 3. The results from different trials were concatenated and separated by the dotted black lines. The MAE of the correlated impedance was  $0.10\pm0.01,~0.08\pm0.02,~0.18\pm0.05,~1.44\pm0.30,~0.84\pm0.27,~1.77\pm0.52,~0.06\pm0.02,~0.02\pm0.00,~0.09\pm0.02$  for  $K_x,~K_{xz},~K_z,~B_x,~B_{zz},~B_z,~J_x,~J_{xz},~and~J_z,~respectively (average and standard deviation calculated across subjects, and normalized by subject mass); where the units for stiffness, damping, and inertia are in N.m/(rad.kg), N.m.s/(rad.kg), and N.m.s²/(rad.kg), respectively. The ranges of impedance variations can be observed in Table I.$ 

TABLE I. MECHANICAL IMPEDANCE OF THE ANKLE GROUPED BY TA MUSCLE CONTRACTION LEVEL. THE IDENTIFIED IMPEDANCE WAS NORMALIZED BY THE SUBJECT MASS, THEN AVERAGED ACROSS SUBJECTS.

TA % MVC	K [(N m)/(rad kg)]			B [(N m s)/(rad kg)] × 10 <sup>-3</sup>			J [(N m s²)/(rad kg)] × 10 <sup>-3</sup>		
	X	XZ	Z	X	XZ	Z	X	XZ	Z
0	$1.00 \pm 0.37$	$0.18 \pm 0.11$	$1.74\pm0.74$	$1.75 \pm 3.46$	$-0.22 \pm 2.05$	$7.30 \pm 3.03$	$0.25\pm0.15$	$-0.02 \pm 0.03$	$0.13\pm0.19$
10	$1.28 \pm 0.44$	$0.24 \pm 0.13$	$2.56\pm0.93$	$3.34 \pm 3.38$	$-0.42 \pm 2.14$	$10.38 \pm 3.72$	$0.29 \pm 0.13$	$-0.02 \pm 0.03$	$0.32 \pm 0.20$
20	$1.24 \pm 0.49$	$0.28 \pm 0.17$	$2.98\pm1.03$	$3.03 \pm 3.48$	$-0.29 \pm 1.74$	$11.73 \pm 4.21$	$0.29 \pm 0.14$	$-0.01 \pm 0.04$	$0.31 \pm 0.15$
30	$1.33 \pm 0.43$	$0.45 \pm 0.22$	$3.75 \pm 1.04$	$3.27 \pm 3.70$	$-0.25 \pm 2.30$	$13.73 \pm 4.58$	$0.31\pm0.14$	$0.00\pm0.04$	$0.42 \pm 0.14$
40	$1.50 \pm 0.51$	$0.58 \pm 0.22$	$4.32\pm1.35$	$3.45\pm3.54$	$-0.02 \pm 1.62$	$17.04 \pm 5.77$	$0.29 \pm 0.19$	$0.01\pm0.03$	$0.58 \pm 0.22$

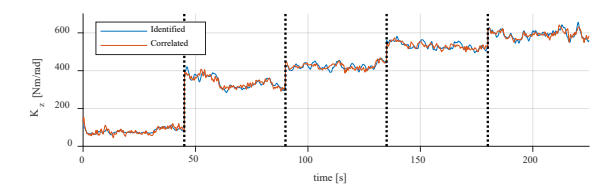


Fig. 3. Identified and correlated ankle stiffness of a representative subject varying within and between trials. The vertical dotted lines separate trials 0%, 10%, 20%, 30%, and 40% MVC, in order.

### IV. DISCUSSION

### A. Directional Ankle Impedance

The ankle impedance showed a high direction-dependency, particularly for the stiffness component. In addition, the cross-axis component was considerable for the stiffness and at higher muscle contraction levels, differently from reported results for the non-loaded ankle [24]. This cross-axis component is responsible for the coupling between the IE and DP anatomical axes, i.e. generating torque in one axis in response to an angle disturbance in the other axis. This behavior can be explained by the muscles in the calf that contribute to motion simultaneously to both the DP and IE directions. Further clinical trials can determine the importance of this coupling for the stability of the ankle.

Possible applications of this finding include a new prosthesis controller design for two active DOF of the ankle. Further demonstration of the benefits of coupled axes for the human gait, may be incorporated into the design of prostheses with an extra degree of freedom of motion in IE (possibly active as in [2]) to emulate the anthropomorphic behavior of the ankle.

### B. Varying Ankle Impedance

To verify that the variations of the identified impedance are caused by the changes in the ankle states rather than by errors of the system identification method, a regression model related the impedance variation to the muscle activity, mean ankle angles, and mean ankle torques. The response of this regression model, named correlated impedance, was compared to the impedance obtained from the system identification method, named identified impedance. The low MAE of each impedance parameter indicated that the changes of muscle activity and ankle kinetics are correlated to the changes in the impedance, suggesting that the observed varying impedance is in fact a response modulated by the subjects, or an effect of fatigue, which can be predicted via EMG signals. Although lower values of MAE were observed in X and XZ components, the Z components varied more substantially across trials (Table I). The lower modulation of IE impedance parameters was also verified in other studies [7], [8].

Note that the angles and torques used for the impedance identification were band-pass filtered between 3 to 20 Hz, while the mean angles and torques used for the impedance prediction were low-pass filtered at 1 Hz. Thus, any noise signal propagated from the kinematic data to the identified impedance could not be propagated from the predictors to the correlated impedance. Therefore, the correlated noise in both the identified and correlated impedance is greatly reduced,

which avoids overestimating the fitness between these two signals. In addition, the calculation of the MAE did not include data samples used for training the correlated impedance model. The low MAE low indicates the model can generalize well to new data, within the ankle conditions of our experimental protocol.

Another possible explanation of the impedance changes in DP and its stiffness components is that these parameters might respond more similarly to a quadratic model than the other parameters. Previous work predicted the ankle impedance from muscle activity using more general models such as Artificial Neural Networks [11], [12], and Gaussian Process Regression models [10]. However, they did not include the ankle angles and ankle torque as the model predictors, which are also relevant variables for impedance modulation [15], [16]. Future work will focus on parameterizing the impedance prediction model using more general models, such as Deep Neural Network, and further use this model to predict the impedance modulation during other ADLs, such as walking or running.

#### C. Limitations

This study has some limitations. First, our subject population was restricted to young males. However, the stiffness is significantly larger in males than in females [25] and the amputee population is substantially older, with 42% of them older than 65 years [26]. Second, our experimental protocol required subjects to control only the TA muscle, while the SOL, PL, and GA were monitored. We opted for this protocol because the subjects could not easily control all four muscles while standing balanced. Finally, even though the subjects could rest between trials, our trial durations of 70 seconds could have fatigued the muscles of some subjects and affected our reported impedance results.

### V.CONCLUSION

This paper derived a mathematical equation for the directional ankle impedance and identified the parameters of the model using experimental data. The model included a term that coupled the IE and DP anatomical axes of the ankle. The stiffness changed by a factor of 1.3 and 2.0 as the muscle activity increased by 30% of the MVC. In addition, the variations of the impedance parameters were explained by changes in the ankle states, which included the mean angle, mean torque, and muscle activity in a single model. The impedance model proposed in this paper presented a high agreement with the experimental data, inferring the ankle torque reaction with subject average VAF above 94%.

As for the application, this work demonstrated theoretically and experimentally that future work identifying the ankle dynamics could account for the interaction between different anatomical axes of the ankle. This work also has implications in new prostheses controller design, which could incorporate a coupling between the control loops of the IE and DP axes.

#### VI. REFERENCES

- [1] S. K. Au, J. Weber, and H. Herr, "Powered Ankle–Foot Prosthesis Improves Walking Metabolic Economy," *IEEE Trans. Robot.*, vol. 25, no. 1, pp. 51–66, Feb. 2009.
- [2] E. M. Ficanha, G. A. Ribeiro, H. Dallali, and M. Rastgaar, "Design and Preliminary Evaluation of a Two DOFs Cable-Driven Ankle-Foot Prosthesis with Active Dorsiflexion-Plantarflexion and Inversion-Eversion," Front. Bioeng. Biotechnol., vol. 4, p. 36, 2016.
- [3] J. D. Ventura, A. D. Segal, G. K. Klute, and R. R. Neptune, "Compensatory mechanisms of transtibial amputees during circular turning," *Gait Posture*, vol. 34, no. 3, pp. 307–312, Jul. 2011.
- [4] H. Lee, E. J. Rouse, and H. I. Krebs, "Summary of human ankle mechanical impedance during walking," *IEEE J. Transl. Eng. Health Med.*, vol. 4, pp. 1–7, 2016.
- [5] A. L. Shorter and E. J. Rouse, "Mechanical Impedance of the Ankle During the Terminal Stance Phase of Walking," *IEEE Trans. Neural* Syst. Rehabil. Eng., vol. 26, no. 1, pp. 135–143, 2018.
- [6] K. R. Embry, D. J. Villarreal, R. L. Macaluso, and R. D. Gregg, "Modeling the Kinematics of Human Locomotion Over Continuously Varying Speeds and Inclines," *IEEE Trans. Neural* Syst. Rehabil. Eng., vol. 26, no. 12, pp. 2342–2350, Dec. 2018.
- [7] H. Lee, P. Ho, M. Rastgaar, H. I. Krebs, and N. Hogan, "Multivariable static ankle mechanical impedance with active muscles," *IEEE Trans. Neural Syst. Rehabil. Eng.*, vol. 22, no. 1, pp. 44–52, 2014.
- [8] H. Lee, H. I. Krebs, and N. Hogan, "Multivariable dynamic ankle mechanical impedance with active muscles," *IEEE Trans. Neural Syst. Rehabil. Eng.*, vol. 22, no. 5, pp. 971–981, 2014.
- [9] E. Ficanha, G. A. Ribeiro, L. Knop, and M. R. Aagaah, "Estimation of the 2-DOF Time-Varying Impedance of the Human Ankle," in 2017 Design of Medical Devices Conference, 2017.
- [10] L. N. Knop, G. A. Ribeiro, and M. Rastgaar, "Towards a Generalized Model of Multivariable Ankle Impedance during Standing based on the Lower Extremity Muscle EMG," presented at the 2019 Design of Medical Devices, Minneapolis, Minnesota, USA, 2019.
- [11] H. Dallali, L. Knop, L. Castelino, E. Ficanha, and M. Rastgaar, "Using lower extremity muscle activity to obtain human ankle impedance in the external-internal direction," *Int. J. Intell. Robot. Appl.*, vol. 2, no. 1, pp. 29–42, 2018.
- [12] H. Dallali, L. Knop, L. Castelino, E. Ficanha, and M. Rastgaar, "Estimating the multivariable human ankle impedance in dorsi-plantarflexion and inversion-eversion directions using EMG signals and artificial neural networks," *Int. J. Intell. Robot. Appl.*, vol. 1, no. 1, pp. 19–31, 2017.
- [13] I. W. Hunter and R. E. Kearney, "Dynamics of human ankle stiffness: variation with mean ankle torque," *J. Biomech.*, vol. 15, no. 10, pp. 747–752, 1982.
- [14] T. E. Sakanaka, J. Gill, M. D. Lakie, and R. F. Reynolds, "Intrinsic ankle stiffness during standing increases with ankle torque and passive stretch of the Achilles tendon," *PloS One*, vol. 13, no. 3, p. e0193850, 2018.
- [15] P. L. Weiss, R. E. Kearney, and I. W. Hunter, "Position dependence of ankle joint dynamics—I. Passive mechanics," *J. Biomech.*, vol. 19, no. 9, pp. 727–735, Jan. 1986.
- [16] P. L. Weiss, R. E. Kearney, and I. W. Hunter, "Position dependence of ankle joint dynamics—II. Active mechanics," *J. Biomech.*, vol. 19, no. 9, pp. 737–751, 1986.
- [17] G. A. Ribeiro, L. N. Knop, and M. Rastgaar, "Correlation Between Ankle Impedance and EMG Signals," in *International Conference on NeuroRehabilitation*, 2018, pp. 627–631.
- [18] L. N. Knop, G. A. Ribeiro, E. M. Ficanha, and M. Rastgaar, "Estimating the Relationship Between Multivariable Standing Ankle Impedance and Lower Extremity Muscle Activation," in 2018 7th IEEE International Conference on Biomedical Robotics and Biomechatronics (Biorob), 2018, pp. 285–290.
- [19] E. M. Ficanha, G. A. Ribeiro, and M. Rastgaar, "Design and evaluation of a 2-dof instrumented platform for estimation of the

- ankle mechanical impedance in the sagittal and frontal planes," *IEEEASME Trans. Mechatron.*, vol. 21, no. 5, pp. 2531–2542, 2016.
- 20] R. H. Byrd, J. C. Gilbert, and J. Nocedal, "A trust region method based on interior point techniques for nonlinear programming," *Math. Program.*, vol. 89, no. 1, pp. 149–185, 2000.
- [21] Abraham. Savitzky and M. J. E. Golay, "Smoothing and Differentiation of Data by Simplified Least Squares Procedures.," *Anal. Chem.*, vol. 36, no. 8, pp. 1627–1639, Jul. 1964.
- [22] C.-Y. Chiu, D. L. Pease, and R. H. Sanders, "The effect of pose variability and repeated reliability of segmental centres of mass acquisition when using 3D photonic scanning," *Ergonomics*, vol. 59, no. 12, pp. 1673–1678, 2016.
- [23] E. J. Rouse, L. J. Hargrove, E. J. Perreault, and T. A. Kuiken, "Estimation of human ankle impedance during the stance phase of walking," *IEEE Trans. Neural Syst. Rehabil. Eng.*, vol. 22, no. 4, pp. 870–878, 2014.
- [24] H. Lee, H. I. Krebs, and N. Hogan, "Multivariable dynamic ankle mechanical impedance with relaxed muscles," *IEEE Trans. Neural Syst. Rehabil. Eng.*, vol. 22, no. 6, pp. 1104–1114, 2014.
- [25] J. Trevino and H. Lee, "Sex Differences in 2-DOF Human Ankle Stiffness in Relaxed and Contracted Muscles," *Ann. Biomed. Eng.*, vol. 46, no. 12, pp. 2048–2056, 2018.
- [26] K. Ziegler-Graham, E. J. MacKenzie, P. L. Ephraim, T. G. Travison, and R. Brookmeyer, "Estimating the prevalence of limb loss in the United States: 2005 to 2050," *Arch. Phys. Med. Rehabil.*, vol. 89, no. 3, pp. 422–429, 2008.